Evaluation of SCEC CyberShake Ground Motions for Engineering Practice

Ganyu Teng,[a] **M.EERI, and Jack Baker,**[a] **M.EERI**

This paper evaluates CyberShake (version 15.12) ground motions for potential application to high-rise building design in the Los Angeles region by comparing them against recordings from past earthquakes as well as empirical models. We consider two selected sites in the Los Angeles region with different underlying soil conditions and select comparable suites of ground motion records from CyberShake and the NGA-West2 database according to the ASCE 7-16 requirements. Major observations include (1) selected ground motions from CyberShake and NGA-West2 share similar features, in terms of response spectra and polarization; (2) when selecting records from CyberShake, it is easy to select motions with sources that match the hazard deaggregation; (3) CyberShake durations on soil are consistent with the empirical models considered, whereas durations on rock are slightly shorter; (4) occasional excessive polarization in ground motion is produced by San Andreas fault ruptures, though those records are usually excluded after the ground motion selection. Results from this study suggest that CyberShake ground motions are a suitable and promising source of ground motions for engineering evaluations. [DOI: 10.1193/100918EQS230M]

INTRODUCTION

Ground motions are used as input for seismic structural analysis and design. Recordings from past earthquakes have served as the main data source for ground motion selection, but the use of simulated ground motion records is also permitted by ASCE/SEI 7-16 (American Society of Civil Engineers 2016). Simulation models have been developed using different methodologies, including stochastic (e.g., Boore 1983, Pousse et al. 2006) and hybrid broadband (e.g., Frankel 2009, Graves and Pitarka 2010, Mai et al. 2010) approaches. Compared to recorded ground motions, simulations provide data for infrequent situations, such as large-magnitude events and ground motions observed on rock sites, close-to-rupture sites, and sites with low seismicity. However, evaluation is necessary to ensure that these simulation outputs are suitable for seismic engineering analysis and design. Analysis of tall buildings is a promising application, as their response is sensitive to long-period excitation (where simulations have the most potential to provide insight) and because tall buildings are typically analyzed using dynamic analysis with ground motion inputs (unlike shorter buildings, which are more often analyzed using simplified static loads).

[a] Department of Civil and Environmental Engineering, Stanford University, Stanford, CA 94305; Email: ganyut@stanford.edu (G. T.)

Earthquake Spectra, Volume 35, No. 3, pages 1311–1328, August 2019; © 2019, Earthquake Engineering Research Institute

Evaluation of simulated ground motions can be performed in a number of ways depending on the ground motion features of interest and intended use of the data (Bradley et al. 2017). A number of studies have evaluated the ability of simulation algorithms to produce realistic response spectra (Aagaard et al. 2008, Frankel 2009, Star et al. 2011, Burks and Baker 2014, Dreger et al. 2015), duration parameters (Hartzell et al. 1999, Afshari and Stewart 2016b), and frequency content (Rezaeian et al. 2015). Others have evaluated simulated ground motions by analyzing the dynamic responses of single-degree-of-freedom structures or multiple-degree-of-freedom structures (Bazzurro et al. 2004, Iervolino et al. 2010, Galasso et al. 2012, 2013, Jayaram and Shome 2012). In particular, Bijelic et al. (2014, 2017, 2018) have conducted evaluations considering nonlinear dynamic responses of high-rise buildings subjected to recorded and simulated ground motions. Past studies have considered different types of simulations, including the Southern California Earthquake Center (SCEC) Broadband Platform (Bijelic et al. 2014, Burks and Baker 2014, Dreger et al. 2015, Burks et al. 2015, Afshari and Stewart 2016b), ShakeOut (Star et al. 2011), and other simulation scenarios (Aagaard et al. 2008, Galasso et al. 2012, 2013, Jayaram and Shome 2012).

CyberShake is a physics-based hybrid broadband ground motion simulation model developed by SCEC (Graves et al. 2011). It is notable for producing unprecedented numbers of simulations, considering all plausible ruptures in the Southern California area. It is also notable for using a three-dimensional crustal velocity model, which provides ground motions with site-specific effects from sedimentary basins and other crustal features of interest when selecting ground motions for engineering analysis. Bijelic et al. (2017) evaluated CyberShake ground motions for predicting nonlinear performance of tall buildings in the Los Angeles region. Besides that study, limited evaluations have been done using CyberShake motions for building analysis, and none have considered building code requirements for selection of motions.

This study evaluates the suitability of CyberShake (version 15.12) simulated ground motions for engineering use in high-rise building analysis in the Los Angeles region. We evaluate simulated ground motions against past earthquake recordings and empirical models. In particular, we select ground motion records for two sites with different underlying soil conditions from CyberShake and NGA-West2 and evaluate several ground motion metrics, including intensity measures, deaggregation, duration, and polarization. Our evaluation process consists of four parts: (1) selecting ground motions from CyberShake and NGA-West2 according to ASCE 7-16 requirements, (2) comparing seismic sources and polarization of the selected ground motions between the two data sources, (3) evaluating CyberShake durations against empirical models, and (4) examining polarization of ground motions generated by CyberShake.

DATA SOURCES

We selected simulated ground motion records from CyberShake (Graves et al. 2011), and recorded ground motions from the NGA-West2 database (Ancheta et al. 2014). CyberShake is a physics-based seismic hazard model that is part of the SCEC Community Modeling Environment and has conducted ground motion simulations in California since 2009.

For this project, we selected ground motions from the latest available simulation (Study 15.12, Study ID = 7), which was conducted for more than 300 sites with 5 km spacing in Southern California, and considered all on-fault ruptures within 200 km from each site as defined in the Uniform California Earthquake Rupture Forecast, Version 2. For each site, there are approximately 7,000 ruptures and 415,000 ground motion time series available. The simulations use the Graves and Pitarka (2015) rupture generator and a hybrid broadband ground motion simulation methodology, which includes a deterministic approach at frequencies below 1 Hz and a stochastic approach at frequencies above 1 Hz. Ground motion time series were accessed via the SCEC servers (SCECpedia 2018).

The NGA-West2 database provides ground motion records from shallow crustal earthquakes worldwide, including 333 global events with magnitudes (M) greater than 5.0 and 266 events in California with magnitudes between 3.0 and 5.45. In total, the database consists of 21,336 ground motion records from earthquakes with magnitudes between 3.0 and 7.9, site-rupture distances (R_{rup}) between 0.05 and 1,533 km, and average shear-wave velocities in the top 30 m of the sites (V_{S30}) between 94 and 2,100 m/s. Ground motion time series were accessed via the NGA-West2 web site (Pacific Earthquake Engineering Research Center (PEER) 2013).

GROUND MOTION SELECTION

ASCE 7-16 GROUND MOTION SELECTION APPROACH

ASCE 7-16 provides requirements for selecting ground motions for engineering analysis in Chapter 16. Similar requirements are provided in other guidance documents, such as the PEER Tall Buildings Initiative Guidelines (PEER 2017). Similar requirements were present in prior versions of the ASCE 7 standard as well. As such, ASCE 7-16 is used as an example to test the broader suitability of CyberShake ground motions to satisfy ground motion selection requirements. The requirements of ASCE 7-16 are based on a target response spectrum, termed the Risk-targeted Maximum Considered Earthquake (MCE_R). This spectrum specifies the amplitude of shaking to be considered and is determined independently of the ground motion selection that is the focus of this study.

Given the MCE_R spectrum, the key requirements of the standard are to select ground motions from earthquakes that are consistent with those controlling the hazard at the site and to select ground motions with response spectra similar to the MCE_R. Specifically, Section 16.2.2 states, "Ground motions shall be selected from events within the same general tectonic regime and having generally consistent magnitudes and fault distances as those controlling the target spectrum and shall have similar spectral shape as the target spectrum… Where the required number of recorded ground motions is not available, it shall be permitted to supplement the available records with simulated ground motions." The latter phrase indicates the historical preference for use of recorded ground motions, but for the example considered here, the importance of large-magnitude earthquakes (of which there are few with appropriate recordings), long-period motions (which are not recorded reliably in older ground motion instruments), and basin effects, means that simulated ground motions are arguably suitable if properly vetted.

SITE SELECTION

We chose two sites with different soil conditions for analysis: Los Angeles downtown (LADT) with a latitude of 34.052, longitude of –118.257, and V_{S30} of 390 m/s; and Pasadena (PAS) with a latitude of 34.148, longitude of –118.171, and V_{S30} of 748 m/s. Their locations are illustrated in Figure 1. For each site we determined a site-specific MCE_R spectrum according to ASCE 7-16 building code requirements. This spectrum was determined using the U.S. Geological Survey (USGS) Unified Hazard Tool (USGS 2018) to find the uniform hazard spectrum with a return period of 2,475 years for the given location and V_{s30}; we then applied a risk coefficient factor of 0.9, representing the risk coefficients obtained from the SEAOC/Office of Statewide Health Planning and Development (OSHPD) Seismic Design Maps (OSHPD 2019) tool. The MCE_R spectra are plotted later in comparison to selected ground motions' spectra.

For the given sites, we assume a building of interest with a 5-s first-mode period. This period, representative of tall buildings built in the region, means that the ground motions selected in the following should match the MCE_R spectrum over the period range of 1 to 10 s (or 0.2 to 2 times the largest first-mode period).

CODE-BASED RECORD SELECTION

We selected 11 pairs of ground motion records from CyberShake and the NGA-West2 database according to ASCE 7-16 building code requirements. Only the two horizontal components of each ground motion were selected. Before selection, we restricted magnitudes and site-rupture distances according to the hazard deaggregation, which reveal the contributions of different sources to the seismic hazard at a site for a given period. Figure 2a, 2b, 2d, and 2e shows the deaggregation results generated using the USGS 2014 hazard analysis at periods of 1 and 5 s with a return period of 2,475 years. The deaggregation results for the two sites are similar, with a major contribution from earthquakes that are within 20 km of the site and have magnitudes from 6.5 to 8. More distant (>40 km) and larger-magnitude ground motions from the San Andreas fault contribute more to the hazard at a period of 5 s than 1 s. Considering these deaggregation results, when selecting records from CyberShake, we considered only

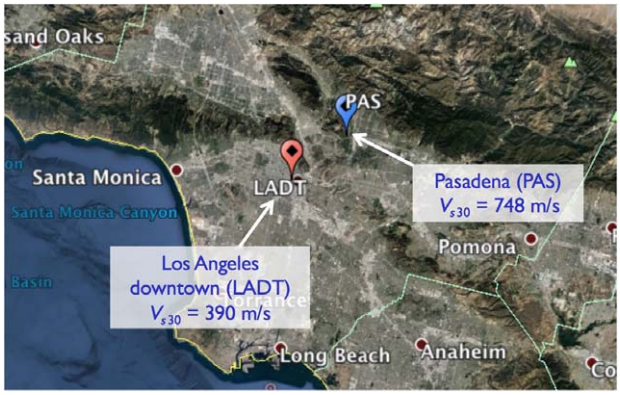

Figure 1. Locations of two selected sites: LADT and PAS. Figure adapted from Google Earth.

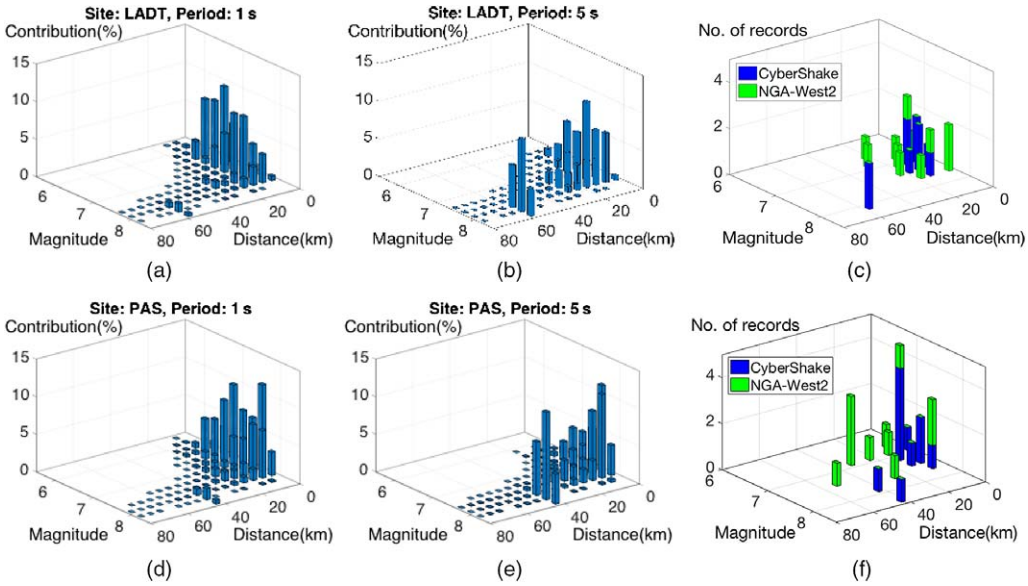

Figure 2. Deaggregation for LADT at (a) 1 s and (b) 5 s; (c) magnitudes and site-rupture distances of selected ground motions for LADT; deaggregation for PAS at (d) 1 s and (e) 5 s; (f) magnitudes and site-rupture distances of selected ground motions for PAS.

simulations for the selected site, took two ground motion records from the San Andreas fault to account for their contribution to hazard (as these were not naturally resulting from the following selection), and did not otherwise constrain the selection. When selecting records from the NGA-West2 database, we considered only recordings from sites with V_{S30} within ± 150 m/s of the target value, with $6 \leq M \leq 8$ and $0 \leq R_{rup} \leq 60$ km.

From the records that satisfied the aforementioned constraints, we then selected 11 records from each database to match the target spectrum from periods between 1 and 10 s. The selected records have the minimum errors of all the available records. Each error is defined as follows:

$$Error_{selected} = \sum_{j} (\ln(Sa_{selected}(T_j)) - \ln(Sa_{targ}(T_j)))^2 \tag{1}$$

where $Sa_{selected}(T_j)$ is the spectral acceleration of the selected record at period T_j, and $Sa_{targ}(T_j)$ is the target spectrum at the same period. The periods used in the CyberShake selection were 22 periods varying from 1 to 10 s, as given in the CyberShake simulation output files. The periods used in the NGA-West2 selection were 38 periods provided in the NGA-West2 database. We allowed no scaling in the CyberShake selection but allowed a maximum scale factor of 4 in the NGA-West2 selection. Maximum direction (RotD100) response spectra were used for both the target spectrum and the candidate record spectra in accordance with ASCE 7-16 guidance. Figure 3 summarizes the response spectra of the sets of 11 selected records in comparison with the target spectra. More detailed documentation of

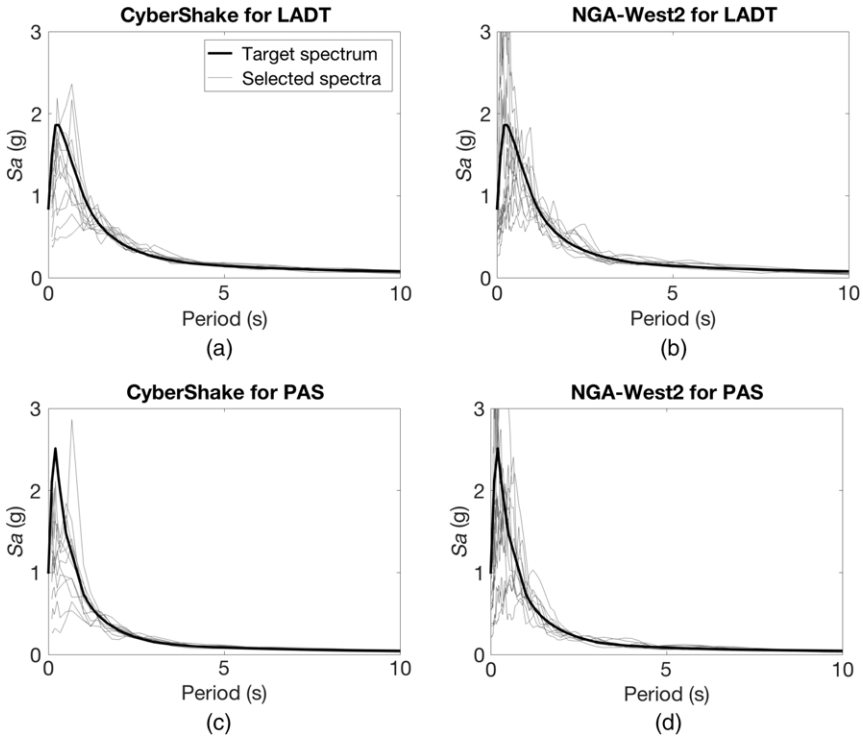

Figure 3. Comparison of the target spectrum and selected response spectra from (a) CyberShake for LADT, (b) NGA-West2 for LADT, (c) CyberShake for PAS, (d) NGA-West2 for PAS.

the selected ground motions, including individual time series and response spectra plots for each ground motion, are provided as an online Appendix.

DEAGGREGATION

Figure 2c and 2f illustrates the magnitudes and site-rupture distances of the selected ground motions from CyberShake and the NGA-West2 database. The magnitudes and site-rupture distances of the 11 CyberShake ground motions are similar to the deaggregation plots from the USGS hazard analysis. The two records from the San Andreas fault are consistent with the 5-s deaggregation plot (Figure 2b and 2e). Other CyberShake ground motions have $R_{rup} < 20$ km and $6.85 \leq M \leq 7.75$, which are consistent with the hazard deaggregation.

Compared to CyberShake ground motions, those selected from the NGA-West2 database have smaller magnitudes: many of them have magnitudes less than 7.0. This is because the NGA-West2 database has a limited number of large-magnitude recordings; a looser match of target magnitudes, combined with use of scaling during the ground motion selection, compensates for this challenge, as is often the case in real-world applications of this procedure. The hazard from larger and more distant earthquakes is not captured by the

11 NGA-West2 ground motions. Overall, it is more difficult to match the hazard deaggregation when selecting ground motions from the NGA-West2 database because of the limited number of recorded earthquakes, even when ground motion scaling is allowed.

POLARIZATION

Polarization refers to the variation in motion intensity as the horizontal orientation of interest varies. Figure 4 illustrates two cases with different degrees of polarization. The peak displacement response in Figure 4a is relatively uniform in the two-dimensional space, whereas the displacement response in Figure 4b is much larger, at an angle of 30°. Polarization is important for engineering practice, in which structures must be able to resist seismic loads in all horizontal orientations, so ground motions with realistic polarization are needed. Here we use $Sa_{RotD100}(T)/Sa_{RotD50}(T)$ to quantify the degree of polarization, where $Sa_{RotD100}(T)$ is the maximum response in all orientations at a given period T, and $Sa_{RotD50}(T)$ is the median response:

$$Sa_{RotD100}(T) = max_{\theta}[Sa(\theta,T)] \tag{2}$$

$$Sa_{RotD50}(T) = median_{\theta}[Sa(\theta,T)] \tag{3}$$

where $Sa(\theta,T)$ denotes the spectral acceleration of a single component of shaking in orientation θ.

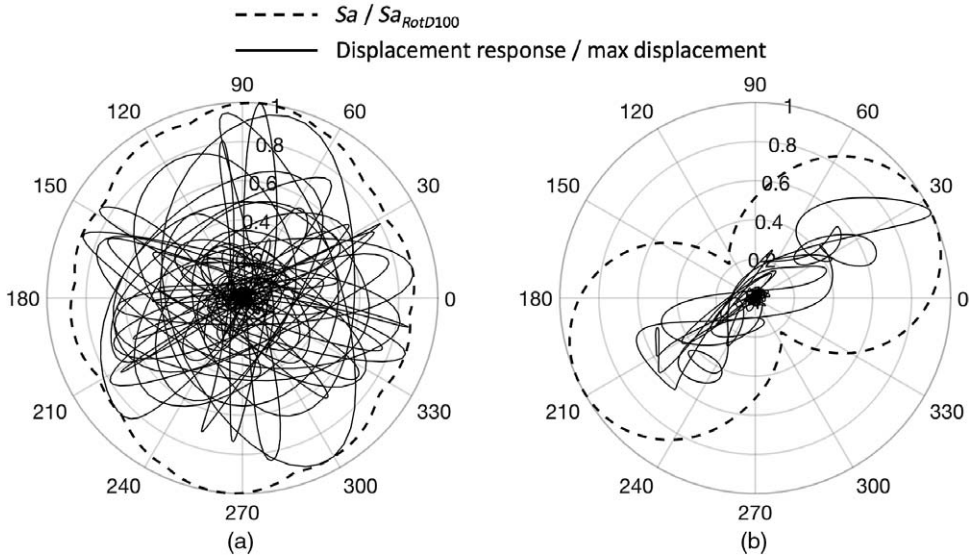

Figure 4. Displacement responses ($T = 1$ s) in all orientations from (a) a not-strongly-polarized ground motion, and (b) a strongly polarized ground motion. The solid line indicates the normalized displacement response over time, and the dashed line indicates the normalized spectral acceleration in the given orientation.

$Sa_{RotD100}(T)/Sa_{RotD50}(T)$ ranges from 1.0 to $\sqrt{2}$, with a larger value indicating a more polarized response; for reference, the ground motion of Figure 4a has a ratio of 1.13, and the ground motion of Figure 4b has a ratio of 1.40. The average value of this metric is relatively stable in recorded ground motions and so is a useful metric for evaluating the reasonableness of the CyberShake simulations (Burks and Baker 2014).

We computed the geometric mean of $Sa_{RotD100}(T)/Sa_{RotD50}(T)$ for the 11 selected ground motion records from two databases and compared it with an empirically calibrated model based on NGA-West2 data (Shahi and Baker 2014). As illustrated in Figure 5, selected motions for both sites from both databases show general agreement with the empirical model and show the general trend of longer periods having larger ratios. While these CyberShake results are satisfactory, there are some limited unusual polarization results that will be discussed later.

GENERAL GROUND MOTION PROPERTIES

The prior section's results indicated that the selected CyberShake ground motions were suitable for use in an ASCE 7-16 analysis, but the results were case-specific, and the generality of the results was unclear. To generalize these findings, several additional studies of the CyberShake ground motions were undertaken and are summarized in the following subsections.

DURATION

Shaking duration can influence the nonlinear responses, cyclic deterioration of strength, and stiffness of structural components (e.g., Hancock and Bommer 2006, Chandramohan et al. 2016). Here we compare 5%–75% significant durations (one of the most common duration metrics) from CyberShake ground motions against three empirical models proposed by Afshari and Stewart (2016a; AS2016), Bommer et al. (2009), and Abrahamson and Silva (1996). All empirical models have common inputs, including magnitudes, site rupture

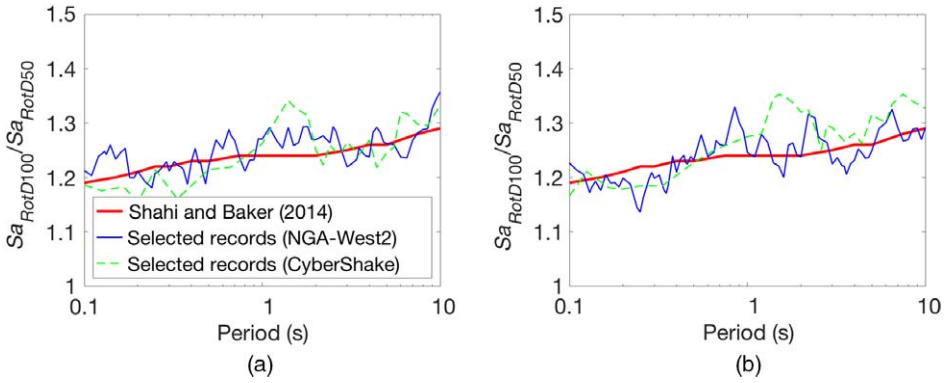

Figure 5. Geometric mean of $Sa_{RotD100}(T)/Sa_{RotD50}(T)$ of the 11 selected ground motions for (a) LADT and (b) PAS, compared to an empirically calibrated model based on NGA-West2 data (Shahi and Baker 2014).

distances, and site soil conditions. Some models have additional inputs. For example, Bommer et al. (2009) takes into account the rupture depth, and AS2016 requires extra inputs of the depth to shear-wave velocity of 1 km/s isosurface and the rupture mechanism. We evaluated the geometric mean values and the dispersion, defined as the log standard deviation, of duration from CyberShake against those from empirical models and examined the effects of magnitudes, site-rupture distances, and underlying soil on durations.

When selecting records from CyberShake, we considered sets of ground motions with R_{rup} values of 20, 50, and 100 km (taking an interval of ± 1 km around those targets when selecting ground motions), and compared their geometric mean duration values with outputs from empirical models. Figure 6 shows the geometric mean values of the >19,000 considered CyberShake motions in comparison with median durations from three empirical models. As illustrated in Figure 6, all curves show the expected trend of larger-magnitude ground motions having longer durations. The effect of the soil and sedimentary basin underlying the LADT site is also reflected in Figure 6: for given R_{rup} and M values, durations observed at LADT are consistently longer than those at PAS.

For LADT, CyberShake durations agree well with empirical models. For PAS, CyberShake durations are somewhat shorter than empirical models. This inconsistency may be in part due to the limited recordings on rock used to constrain the empirical models (for example, the NGA-West2 database has 230 recordings with $19 \leq R_{rup} \leq 21$ km

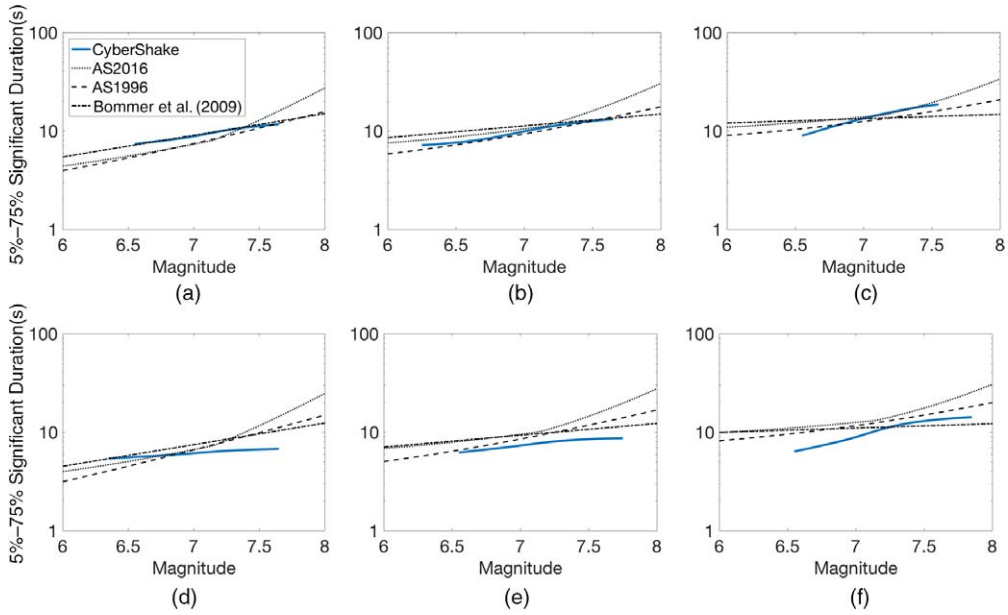

Figure 6. Geometric mean durations for LADT with R_{rup} of (a) 20 km, (b) 50 km, and (c) 100 km in comparison with the median values from empirical models. Geometric mean durations for PAS with R_{rup} of (d) 20 km, (e) 50 km, and (f) 100 km in comparison with the median values from empirical models. AS1996 = Abrahamson and Silva (1996); AS2016 = Afshari and Stewart (2016a).

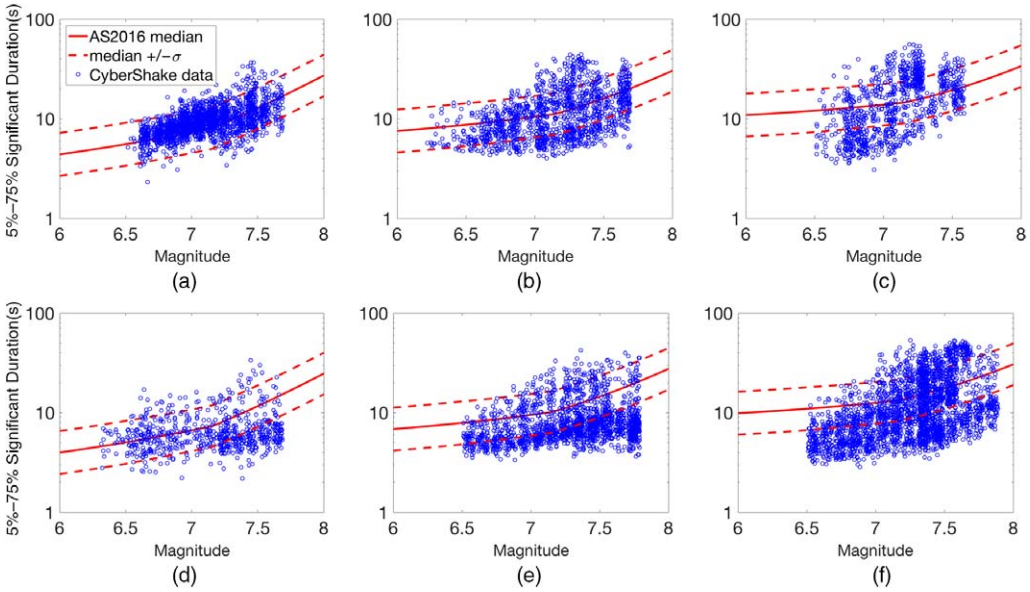

Figure 7. Duration observations from CyberShake, plotted versus magnitude, for several R_{rup} ranges. AS2016 predictions are also plotted for reference. (a) LADT with $19 \leq R_{rup} \leq 21$ km, (b) LADT with $49 \leq R_{rup} \leq 51$ km, (c) LADT with $99 \leq R_{rup} \leq 101$ km, (d) PAS with $19 \leq R_{rup} \leq 21$ km, (e) PAS with $49 \leq R_{rup} \leq 51$ km, and (f) PAS with $99 \leq R_{rup} \leq 101$ km.

and $240 \leq V_{S30} \leq 540$ m/s, almost 4 times more than the number of recordings with the same R_{rup} and $600 \leq V_{S30} \leq 1{,}800$ m/s). For both sites, the increasing difference between CyberShake and empirical models at larger magnitudes can be explained by the lack of observed earthquakes with $M > 7.5$, leading to larger epistemic uncertainties in the empirical models (Afshari and Stewart 2016a).

Figure 7 illustrates the distribution of durations from CyberShake plotted against the AS2016 median curve (solid red line) and the one-standard-deviation range (dotted red line). For clarity, we plot only half of the CyberShake data and label their magnitudes as the original values plus a random number between –1/60 and 1/60 (to eliminate the vertical banding of the data). For a given R_{rup}, the dispersion from the empirical model stays relatively constant with different magnitudes, whereas the dispersion from CyberShake varies as magnitudes vary. There is a large fraction of CyberShake durations lying more than one standard deviation away from the median curve. This is more significant at PAS, where most CyberShake durations are more than one standard deviation below the median curve. This suggests that CyberShake generates much shorter durations on rock compared with the empirical model. Moreover, we observed a source-specific effect generated from CyberShake by constructing the scatter plots. As illustrated in Figure 8, some sources (marked in blue triangles) generate longer durations compared to others. For example, San Joaquin Hills and Coronado Bank, marked in blue triangles in Figure 8a and 8b,

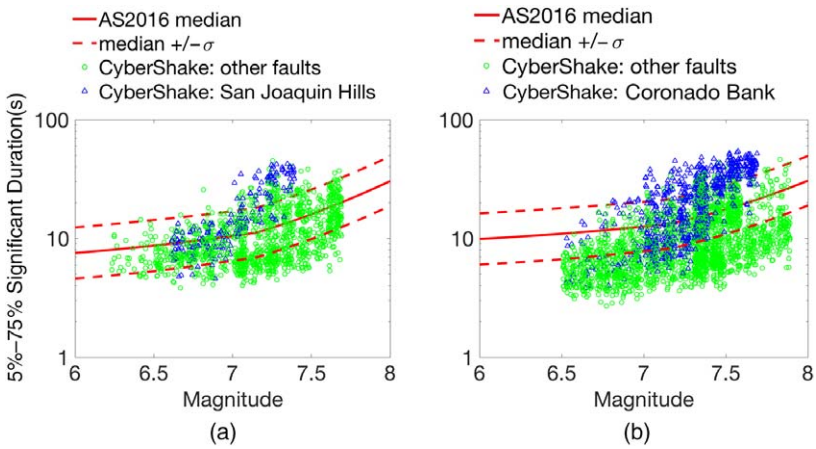

Figure 8. Durations for (a) LADT with $49 \leq R_{rup} \leq 51$ km, and (b) PAS with $99 \leq R_{rup} \leq 101$ km.

respectively, generate ground motions with longer durations compared to other sources at similar R_{rup}. This source-specific effect cannot be reflected by empirical models.

POLARIZATION

We analyzed polarization effects generated by CyberShake and explored the impact of magnitudes, site-rupture distances, site-rupture orientations, and epicenter locations on response spectra polarization. Figure 9 illustrates ground motions for several rupture-site cases. For each case, we selected two events with different epicenters, one close to the site and one far from the site, and plotted their locations and corresponding velocity seismograms. The first and third columns show the location of sites (marked as circles), surface projection of faults (marked as polygons), and epicenters (marked as stars). The second and fourth columns are their corresponding velocity seismograms. The last column shows the geometric mean $Sa_{RotD100}(T)/Sa_{RotD50}(T)$ of all events with the given rupture-site pair, where the red line is the geometric mean value from CyberShake. These geometric mean values are based on between 50 and 270 ground motions (depending on the case), so they indicate more general trends to supplement the anecdotal information in the other columns. The blue dashed line is a prediction based on data from the NGA-West2 database (Shahi and Baker 2014). We considered three R_{rup} ranges (<3, 30, and 50 km) and three magnitudes (7.05, 7.45, and 7.75). For a given rupture, we considered two sites with the same R_{rup} but different site-rupture orientations (perpendicular and parallel to the rupture).

Considering Cases 1 through 4, we observe that for a given R_{rup}, ground motions recorded at sites perpendicular to the rupture (Cases 1 and 2) are less polarized than those at sites parallel to the fault (Cases 3 and 4). In Cases 3 and 4, highly polarized seismograms are observed at sites off the end of the fault. Some polarization of ground motion is observed at near-fault sites (caused by radiation patterns) and down-rupture sites (caused by

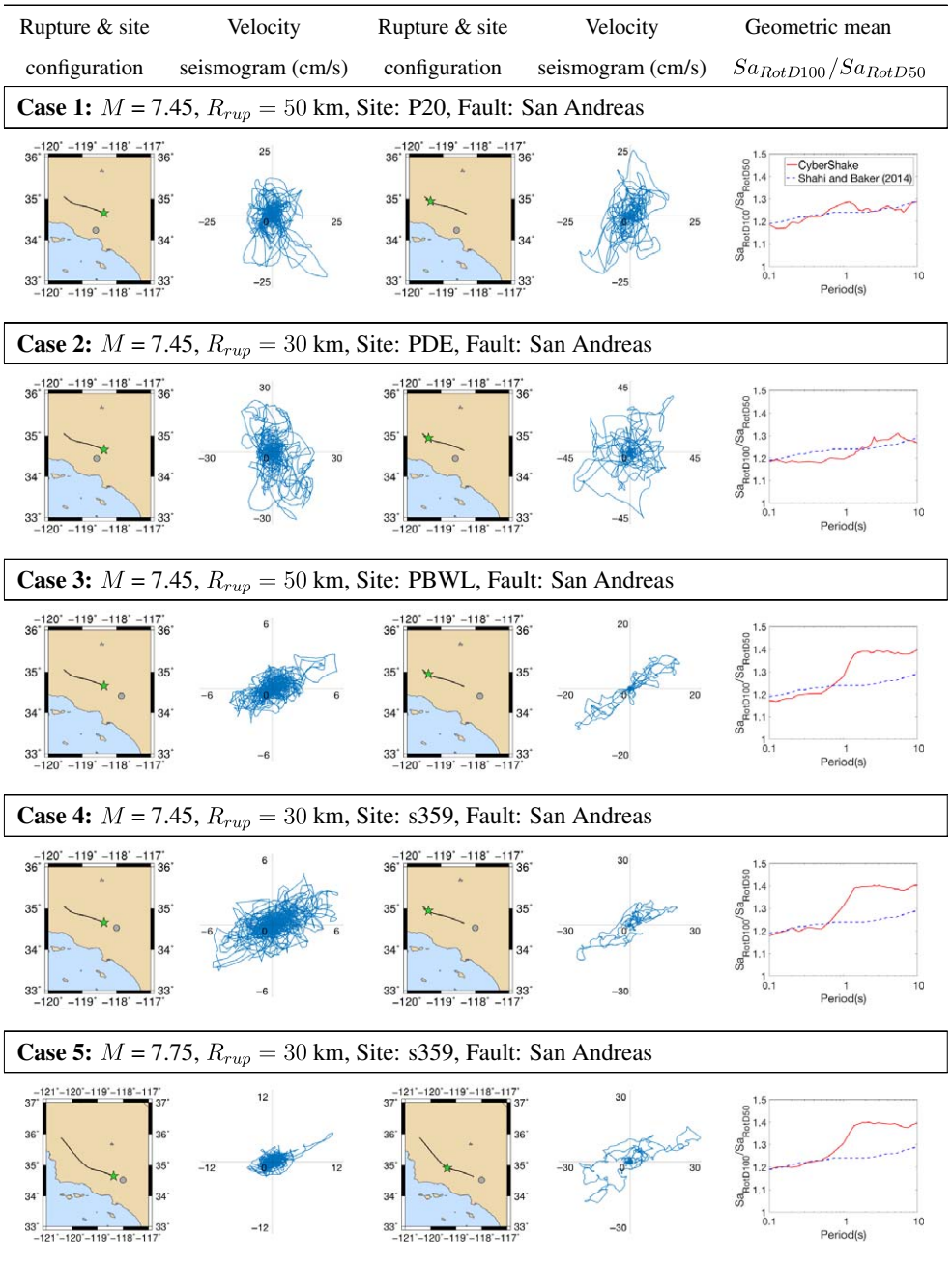

Figure 9. Ground-motion polarization from nine rupture-site cases: (a) cases 1 through 5; (b) cases 6 through 9. Columns 1 and 3 show rupture and site configuration; columns 2 and 4 show their corresponding velocity seismograms, with the *x*-axis representing the E-W direction and the *y*-axis representing the N-S direction; Column 5 shows the geometric mean of all events given a rupture-site pair (the red line) and an empirical model of the anticipated geometric mean for reference (the blue dashed line).

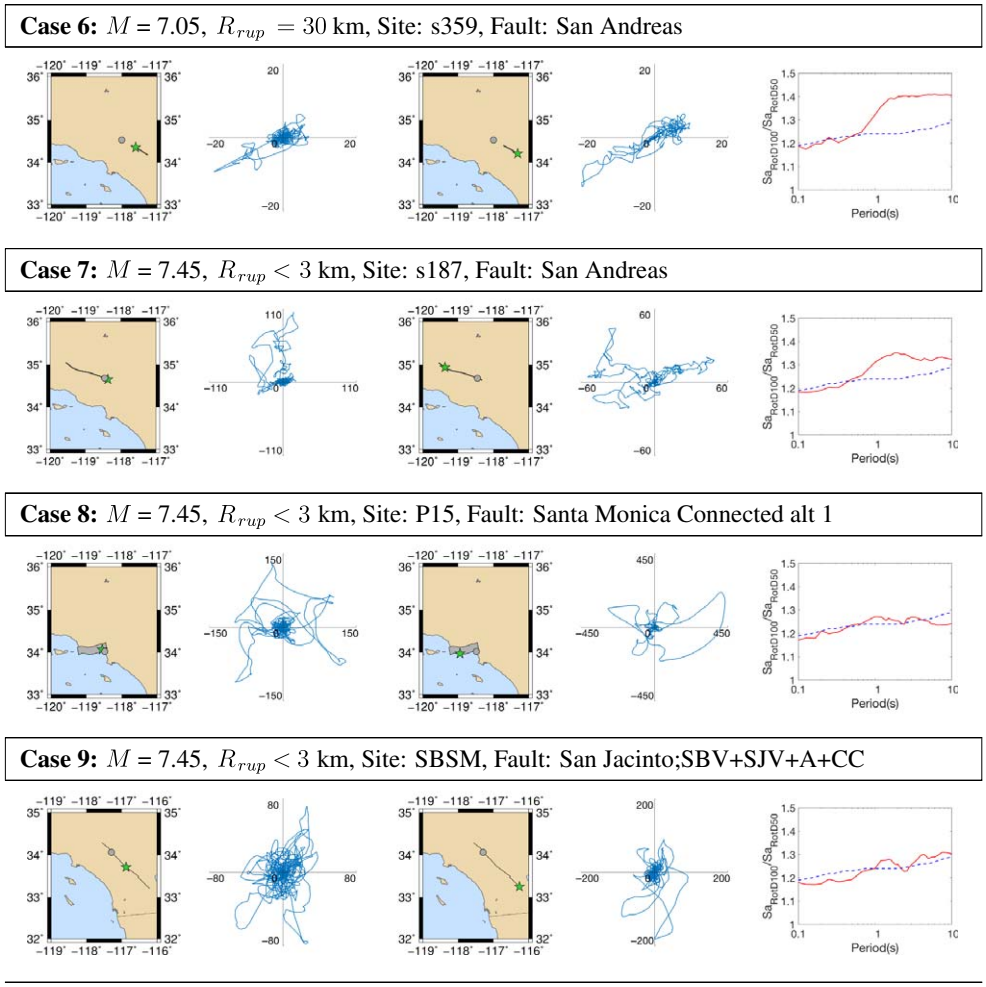

(b)

Figure 9. *Continued.*

directivity), but such polarization is rarely seen in empirical recordings in conditions like these where $R_{rup} \geq 30$ km (Somerville et al. 1997, Watson-Lamprey and Boore 2007).

Further considering Cases 1 through 4, we observe that at sites parallel to the rupture (Cases 3 and 4), when the epicenter is farther away from the site, the velocity seismogram is more polarized. For these two cases, the change in $Sa_{RotD100}(T)/Sa_{RotD50}(T)$ can reach up to 0.038 for $T < 1$s. This difference is negligible, however, at sites perpendicular to ruptures (Cases 1 and 2).

Considering cases with the same site and fault but differing magnitudes (Cases 4 through 6), we find that magnitude has a negligible effect on the polarization. In these cases, all geometric mean $Sa_{RotD100}(T)/Sa_{RotD50}(T)$ curves have high polarization at periods longer than 1 s.

We also observed occasional excessive polarization in ground motions generated by the San Andreas fault. Given a site-rupture distance, site-rupture orientation, and magnitude, ground motions generated from the San Andreas fault (Case 7) are more polarized compared to those from an inclined fault (Santa Monica, Case 8) as well as another strike-slip fault (San Jacinto, Case 9). The geometric mean $Sa_{RotD100}(T)/Sa_{RotD50}(T)$ of ground motions from the San Andreas fault can be more than 0.1 larger than the average geometric mean of observed ratios from the NGA-West2 database (Shahi and Baker 2014). However, differences between the average geometric means and curves from other faults (Case 8 and 9) are within 0.05. Moreover, $Sa_{RotD100}(T)/Sa_{RotD50}(T)$ plots in Cases 3 to 7 address a strong frequency dependence of polarization effect generated by the San Andreas fault, with periods longer than 1 s showing relatively high $Sa_{RotD100}(T)/Sa_{RotD50}(T)$ values. As illustrated in these plots, the geometric mean $Sa_{RotD100}(T)/Sa_{RotD50}(T)$ increases significantly at 1 s and stays relatively constant after 1 s.

The degree of polarization for $T > 1$s in several of these cases is much greater than anything seen in empirical data sets. Furthermore, the transition from low to high polarization at $T = 1$s coincides with the transition between the deterministic ground motion simulation methodology and the stochastic approach. For these reasons, we believe the excessive polarization to be an artifact of the simulation procedure rather than an indicator of some physical phenomenon. A new version of a rupture generator developed by Graves and Pitarka (2016) may address these issues by incorporating stronger spatial and temporal heterogeneity to reduce the coherence of radiated energy as well as making a smoother and more realistic transition at 1 s (Robert Graves, *pers. comm.*). Although we observed occasional excessive polarization generated by CyberShake, it should be emphasized that these cases are relatively rare among the overall database of simulations (less than 2%), and those highly polarized records can easily be excluded during ground motion selection; they were naturally omitted from the record selection in this study without any special effort to do so, and they could also be easily excluded through an additional polarization check during the search procedure.

CONCLUSIONS

This study evaluated the use of CyberShake (version 15.12) ground motion simulations for engineering application in tall building design. An engineering practice–oriented process was used to evaluate simulated ground motions as compared to recordings from real earthquakes and empirical ground motion models. We studied four ground motion metrics: intensity measures, deaggregation, duration, and polarization effect.

We selected ground motions satisfying ASCE 7-16 requirements from CyberShake and NGA-West2. LADT and PAS sites, with differing underlying soil conditions, were considered. The target spectrum was computed using a site-specific MCE_R spectrum, and 11 ground motion records were identified to match the target spectrum at periods between 1 and 10 s.

The magnitudes and site-rupture distances of selected ground motions were compared against hazard deaggregation from the USGS 2014 hazard analysis, with a return period of 2,475 years. The comparisons showed that seismic sources of the selected CyberShake ground motions were consistent with USGS deaggregation results, whereas the selected NGA-West2 records had smaller magnitudes. When selecting ground motions from CyberShake, we were able to restrict magnitudes, site-rupture distances, and sources to match the

hazard deaggregation because of the large data size. This was difficult when selecting ground motions from the NGA-West2 database because of the limited records from real earthquakes.

We compared CyberShake durations against three empirical models: Afshari and Stewart (2016a), Bommer et al. (2009), and Abrahamson and Silva (1996). Some similar patterns were observed for all sources: (1) for a given R_{rup}, larger magnitudes resulted in longer durations; and (2) durations observed on soil were consistently longer than those on rock. Overall, results from CyberShake at the soil site (LADT) matched well with empirical models for $M < 7.5$. For the rock site (PAS), most CyberShake durations were shorter than the empirical models' outputs. The inconsistency could be partly due to limited records of large events or on rock sites.

We compared the polarization effect of the 11 selected ground motions with the average observed values in the NGA-West2 database (Shahi and Baker 2014) and found that their geometric mean $Sa_{RotD100}/Sa_{RotD50}$ values were consistent with the average ratios in Shahi and Baker (2014). We also analyzed polarization effects generated by CyberShake in detail and explored the impact of magnitudes, site-rupture distances, site-rupture orientations, and epicenter locations on the polarization of ground motion. Some observations included the following: (1) the effect of magnitude on polarization was negligible; (2) given a R_{rup}, ground motions recorded at sites perpendicular to the fault were less polarized than those at sites parallel to the fault; and (3) the effect of epicenter location on the polarization effect was more significant for sites along the fault. Moreover, we also observed occasional excessive polarization in ground motions generated by the San Andres fault. It produced a strong frequency dependence of polarization effect, with periods longer than 1 s showing relatively high $Sa_{RotD100}/Sa_{RotD50}$ values. This was partially caused by the transition from deterministic ground motion simulation methodology to the stochastic approach at 1 s. These records with strong frequency dependence of polarization were usually excluded after ground motion selection.

In conclusion, we analyzed a number of ground motion metrics to provide further insights regarding the value of physics-based ground motion simulations for engineering use. The results suggested that in the considered cases, the ground motions from the CyberShake and the NGA-West2 database were suitable for satisfying ASCE 7-16 requirements. While some CyberShake ground motions appeared to have excessive polarization, this did not affect the example ground motion selection, and a simple check could be used to avoid such ground motions in other selection exercises. More promisingly, the CyberShake database could easily provide ground motions with appropriate earthquake magnitudes and site-rupture distances (because of its vast number of simulations and because, by definition, simulations have been produced for all relevant faults in the region). For these reasons, we conclude that CyberShake is a suitable and promising source of ground motions for engineering evaluations.

ACKNOWLEDGMENTS

We thank Scott Callaghan for help in accessing the CyberShake database, and Robert Graves for feedback on some results. This research was supported by SCEC (Contribution Number 8224). SCEC is funded by National Science Foundation Cooperative Agreement EAR-1033462 and USGS Cooperative Agreement G12AC20038.

APPENDIX

Please refer to the online version of this manuscript to access the supplementary material showing CyberShake and NGA-West2 ground motions for Southern California sites, which is provided in the Appendix.

REFERENCES

Aagaard, B. T., Brocher, T. M., Dolenc, D., Dreger, D., Graves, R. W., Harmsen, S., Hartzell, S., Larsen, S., McCandless, K., Nilsson, S., Petersson, N. A., Rodgers, A., Sjögreen, B., and Zoback, M. L., 2008. Ground-motion modeling of the 1906 San Francisco earthquake, part II: Ground-motion estimates for the 1906 earthquake and scenario events, *Bulletin of the Seismological Society of America* **98**, 1012–1046.

Abrahamson, N., and Silva, W., 1996. *Empirical Ground Motion Models*, report to Brookhaven National Laboratory, Upton, NY.

Afshari, K., and Stewart, J. P., 2016a. Physically parameterized prediction equations for significant duration in active crustal regions, *Earthquake Spectra* **32**, 2057–2081.

Afshari, K., and Stewart, J. P., 2016b. Validation of duration parameters from SCEC broadband platform simulated ground motions, *Seismological Research Letters* **87**, 1355–1362.

American Society of Civil Engineers, 2016. *Minimum Design Loads for Buildings and Other Structures*, ASCE 7-16, Reston, VA.

Ancheta, T. D., Darragh, R. B., Stewart, J. P., Seyhan, E., Silva, W. J., Chiou, B. S. -J., Wooddell, K. E., Graves, R. W., Kottke, A. R., Boore, D. M., Kishida, T., and Donahue, J. L., 2014. NGA-West2 database, *Earthquake Spectra* **30**, 989–1005.

Bazzurro, P., Sjoberg, B., and Luco, N., 2004. Post-elastic response of structures to synthetic ground motions, *Report for Pacific Earthquake Engineering Research (PEER) Center Lifelines Program Project*, Berkeley, CA, 65–112.

Bijelic, N., Lin, T., and Deierlein, G., 2014. Seismic response of a tall building to recorded and simulated ground motions, SCEC Contribution #1930, in *Proceedings, Tenth U.S. National Conference on Earthquake Engineering*, Earthquake Engineering Research Institute, Anchorage, AK.

Bijelic, N., Lin, T., and Deierlein, G., 2017. Utilization of CyberShake earthquake simulations for building performance assessment, in *Proceedings, 16th World Conference on Earthquake Engineering*, 09–13 January, Santiago, Chile.

Bijelic, N., Lin, T., and Deierlein, G. G., 2018. Validation of the SCEC Broadband Platform simulations for tall building risk assessments considering spectral shape and duration of the ground motion, *Earthquake Engineering & Structural Dynamics* **47**, 2233–2251.

Bommer, J. J., Stafford, P. J., and Alarcón, J. E., 2009. Empirical equations for the prediction of the significant, bracketed, and uniform duration of earthquake ground motion, *Bulletin of the Seismological Society of America* **99**, 3217–3233.

Boore, D. M., 1983. Stochastic simulation of high-frequency ground motions based on seismological models of the radiated spectra, *Bulletin of the Seismological Society of America* **73**, 1865–1894.

Bradley, B. A., Pettinga, D., Baker, J. W., and Fraser, J., 2017. Guidance on the utilization of earthquake-induced ground motion simulations in engineering practice, *Earthquake Spectra* **33**, 809–835.

Burks, L. S., and Baker, J. W., 2014. Validation of ground-motion simulations through simple proxies for the response of engineered systems, *Bulletin of the Seismological Society of America* **104**, 1930–1946.

Burks, L. S., Zimmerman, R. B., and Baker, J. W., 2015. Evaluation of hybrid broadband ground motion simulations for response history analysis and design, *Earthquake Spectra* **31**, 1691–1710.

Chandramohan, R., Baker, J. W., and Deierlein, G. G., 2016. Impact of hazard-consistent ground motion duration in structural collapse risk assessment, *Earthquake Engineering & Structural Dynamics* **45**, 1357–1379.

Dreger, D. S., Beroza, G. C., Day, S. M., Goulet, C. A., Jordan, T. H., Spudich, P. A., and Stewart, J. P., 2015. Validation of the SCEC broadband platform V14.3 simulation methods using pseudospectral acceleration data, *Seismological Research Letters* **86**, 39–47.

Frankel, A., 2009. A constant stress-drop model for producing broadband synthetic seismograms: Comparison with the next generation attenuation relations, *Bulletin of the Seismological Society of America* **99**, 664–680.

Galasso, C., Zareian, F., Iervolino, I., and Graves, R., 2012. Validation of ground-motion simulations for historical events using SDoF systems, *Bulletin of the Seismological Society of America* **102**, 2727–2740.

Galasso, C., Zhong, P., Zareian, F., Iervolino, I., and Graves, R. W., 2013. Validation of ground-motion simulations for historical events using MDoF systems, *Earthquake Engineering & Structural Dynamics* **42**, 1395–1412.

Graves, R., Jordan, T. H., Callaghan, S., Deelman, E., Field, E., Juve, G., Kesselman, C., Maechling, P., Mehta, G., Milner, K., Okaya, D., Small, P., and Vahi, K., 2011. CyberShake: A physics-based seismic hazard model for Southern California, *Pure and Applied Geophysics* **168**, 367–381.

Graves, R. W., and Pitarka, A., 2010. Broadband ground-motion simulation using a hybrid approach, *Bulletin of the Seismological Society of America* **100**, 2095–2123.

Graves, R., and Pitarka, A., 2015. Refinements to the Graves and Pitarka (2010) broadband ground-motion simulation method, *Seismological Research Letters* **86**, 75–80.

Graves, R., and Pitarka, A., 2016. Kinematic ground-motion simulations on rough faults including effects of 3D stochastic velocity perturbations, *Bulletin of the Seismological Society of America* **106**, 2136–2153.

Hancock, J., and Bommer, J. J., 2006. A state-of-knowledge review of the influence of strong-motion duration on structural damage, *Earthquake Spectra* **22**, 827–845.

Hartzell, S., Harmsen, S., Frankel, A., and Larsen, S., 1999. Calculation of broadband time histories of ground motion: Comparison of methods and validation using strong-ground motion from the 1994 Northridge earthquake, *Bulletin of the Seismological Society of America* **89**, 1484–1504.

Iervolino, I., De Luca, F., and Cosenza, E., 2010. Spectral shape-based assessment of SDOF nonlinear response to real, adjusted and artificial accelerograms, *Engineering Structures* **32**, 2776–2792.

Jayaram, N., and Shome, N., 2012. A statistical analysis of the response of tall buildings to recorded and simulated ground motions, in *Proceedings, 15th World Conference on Earthquake Engineering*, 24–28 September, Lisbon, Portugal, 1–10.

Mai, P. M., Imperatori, W., and Olsen, K. B., 2010. Hybrid broadband ground-motion simulations: Combining long-period deterministic synthetics with high-frequency multiple S-to-S backscattering, *Bulletin of the Seismological Society of America* **100**, 2124–2142.

Office of Statewide Health Planning and Development (OSHPD), 2019. U.S. seismic design maps, available at https://seismicmaps.org/ (last accessed May 2019).

Pacific Earthquake Engineering Research Center (PEER), 2013. PEER Ground Motion Database, available at https://ngawest2.berkeley.edu/ (last accessed August 2018).

Pacific Earthquake Engineering Center (PEER), 2017. *Guidelines for Performance-Based Seismic Design of Tall Buildings Version 2.0*, Report No. 2017/06, Berkeley, CA.

Pousse, G., Bonilla, L. F., Cotton, F., and Margerin, L., 2006. Nonstationary stochastic simulation of strong ground motion time histories including natural variability: Application to the K-net Japanese database, *Bulletin of the Seismological Society of America* **96**, 2103–2117.

Rezaeian, S., Zhong, P., Hartzell, S., and Zareian, F., 2015. Validation of simulated earthquake ground motions based on evolution of intensity and frequency content, *Bulletin of the Seismological Society of America* **105**, 3036–3049.

SCECpedia, 2018. Accessing CyberShake seismograms, available at https://scec.usc.edu/scecpedia/Accessing_CyberShake_Seismograms (last accessed September 2018).

Shahi, S. K., and Baker, J. W., 2014. NGA-West2 models for ground motion directionality, *Earthquake Spectra* **30**, 1285–1300.

Somerville, P. G., Smith, N. F., Graves, R. W., and Abrahamson, N. A., 1997. Modification of empirical strong ground motion attenuation relations to include the amplitude and duration effects of rupture directivity, *Seismological Research Letters* **68**, 199–222.

Star, L. M., Stewart, J. P., and Graves, R. W., 2011. Comparison of ground motions from hybrid simulations to NGA prediction equations, *Earthquake Spectra* **27**, 331–350.

U.S. Geological Survey (USGS), 2018. Unified Hazard Tool, available at https://earthquake.usgs.gov/hazards/interactive/ (last accessed April 2018).

Watson-Lamprey, J. A., and Boore, D. M., 2007. Beyond SaGMRotI: Conversion to SaArb, SaSN, and SaMaxRot, *Bulletin of the Seismological Society of America* **97**, 1511–1524.

(Received 9 October 2018; Accepted 31 January 2019)